# Single-cell analysis of uterosacral ligament revealed cellular heterogeneity in women with pelvic organ prolapse

**Xiaochun Liu** ( tyxchliu@163.com )
Shanxi Bethune Hospital
**Minna Sue**
**Lingyun Wei**
**Jia Zhang**
**Wenzhen Wang**
**Qian Hao**
**Xiling Lin**
**Lili Wang**

**Article**

**Keywords:**

**Posted Date:** March 14th, 2023

**DOI:** https://doi.org/10.21203/rs.3.rs-2627604/v1



**Additional Declarations:** There is **NO** Competing Interest.

**Version of Record:** A version of this preprint was published at Communications Biology on February 7th, 2024. See the published version at https://doi.org/10.1038/s42003-024-05808-3.

# Abstract

Pelvic organ prolapse (POP) markedly affects the quality of life of women, including significant financial burden. Different cell types and corresponding marker genes were identified in the vaginal wall of women with POP; however, no study has explored gene expression and cellular heterogeneity in the uterosacral ligament. Using single-cell RNA sequencing, we constructed a transcriptional profile of the uterosacral ligament and control samples, and identified 10 major cell types. We performed subpopulation analysis of POP primary cells, explored differentially expressed genes, and performed pseudo-time and transcription factor analyses. We verified previous cell clusters of human fibroblasts, neutrophils, and found new clusters of uterosacral ligaments. Additionally, we dissected pattern changes of cell–cell interaction between stromal and immune cells and transcription factors related to the extracellular matrix, development, and immunity in POP. Here we provide insight into the molecular mechanisms of POP and valuable information for future research directions.


# Introduction

Pelvic organ prolapse (POP) is the displacement of female pelvic organs (vagina, bladder, uterus, and/or rectum) caused by the weakness of their associated supporting tissue. It is a prevalent, burdensome, and limiting disease with enormous physical and emotional discomfort and a huge economic burden [1,2]. The prevalence of POP is 3–6% worldwide [3], 19.7% in 16 developing countries [4,5], 9.67% in China [5], and 2.9% in the USA [6]. With increased longevity, it is expected that the prevalence of symptomatic POP will increase to 46% by the year 2050 in the USA [7]. Up to 29.2% of the patients who undergo prolapse surgery will undergo another surgery for genital prolapse [8]. POP is associated with age, parity, body mass index, hormonal status, diabetes, social factors, genetic predisposition, and obstetric factors [1,9,10]. However, the pathophysiology of POP remains unclear, and risk factors fail to explain the mechanism of the occurrence and development of POP without risk factors.

The uterosacral ligaments (USL) play indispensable roles in apical support of the uterus and upper vagina in POP [11,12]. Unlike the skeletal ligaments that connect the bones, USL is a visceral ligament similar to the mesenteries and is composed of smooth muscle, blood vessels, nerves, adipose tissue, and loose connective tissue [13]. Substantial evidence suggests that the pathophysiological mechanisms underlying POP are related to changes in the extracellular matrix (ECM) of supporting tissues. The USL is mainly composed of the ECM [14]. Histological studies of USL in patients with POP have shown that both types I and III collagen are reduced with an increased III/I ratio, and the ECM density is reduced [14–17]. Moreover, it has been reported that the expression of the collagen-degrading enzyme, matrix metalloproteinase (MMP), is increased, and the expression of the tissue inhibitor of metalloproteinases (TIMP) is decreased, indicating dysregulation of MMP and TIMP [14,18]. In addition, studies have shown that the increased infiltration of neutrophils in the USL is related to the occurrence of POP [19,20]. Numerous studies have reported proteomic, transcriptomic, and genomic changes in POP [14,18–23]. At the gene level,

complex pathogenesis is believed to be involved in POP, including those related to changes in the ECM, immune responses, signaling pathways, and differentially expressed genes [24–26].

A powerful approach for high-resolution transcriptomics analysis is single-cell RNA sequencing (scRNA-seq), which provides an opportunity to decipher the heterogeneity of gene expression in individual cell populations. Although Li et al. [21] have used scRNA-seq to construct a transcriptomic atlas of anterior vaginal prolapse in POP using the vaginal wall and contributed to defining the molecular mechanism of POP, no study has analyzed the gene expression changes of the USL in POP by performing scRNA-seq thus far. Hence, this study aimed to provide a transcriptomic atlas for normal and prolapsed human USL cell types, identify differentially expressed genes in different cell types of the USL, and construct a differentiation trajectory of the primary cells. In addition, we analyzed the intercellular communication and key transcription factors (TFs) in USL. The role of USL cells in ECM remodeling and the immune response was revealed. We provided a molecular mechanism for prolapse at the single-cell level and enhanced the understanding of the pathophysiological process of POP, providing insight to improve current prevention and treatment strategies.

## Results

# Single-cell transcriptomic atlas in POP and control samples

To dissect the cellular heterogeneity and expression characteristics of USL in patients with POP, we performed scRNA sequencing of the USL in three patients with POP and one control patient who had undergone hysterectomy for hysteromyoma (Fig. 1A). After strict quality control, we obtained the transcriptomes of 30,452 single cells. Using dimension reduction and unsupervised graph clustering, we obtained 10 cell subpopulations (Fig. 1B). According to at least three well-known cell markers, including COL1A1, COL1A2, and DCN for fibroblasts, the cells were annotated into 10 cell types: smooth muscle cells (34.93%), endothelial cells (21.29%), fibroblasts (17.36%), neutrophils (4.92%), macrophages (5.36%), monocytes (4.05%), mast cells (4.05%), T cells (3.70%), B cells (0.85%), and dendritic cells (DCs) (0.94%) (Fig. 1C, Supplementary Fig. 1). The three most abundant cell types were smooth muscle cells, endothelial cells, and fibroblasts. The ratio of fibroblasts and smooth muscle cells in the POP group was similar to that in control group, suggesting that abnormal gene expression may be more crucial than the ratio change. Compared to the control group, the number of macrophages, neutrophils, and mast cells in the POP group increased, and the number of endothelial cells decreased significantly, suggesting that these cells play a role in the pathophysiological mechanisms of POP (Fig. 1D).

To understand the functions of each cell type in the USL, we analyzed the top 10 differentially expressed genes (DEGs) (Fig. 1E) and performed Gene Ontology (GO) function enrichment analysis (Supplementary Fig. 2). Smooth muscle cells (SMCs) are enriched in mitochondrial pathways, whereas extracellular matrix pathways are downregulated in monocytes, mast cells, DCs, and T cells. In addition, to understand the changes in expressed genes in the POP group compared with the control group, we examined the differentially expressed genes in all cell types. Compared with the control group, the specific up- and

downregulated genes of each cell type in the POP group are shown in the volcano plot (Fig. 1F). The enrichment analysis revealed that, compared with the control samples, the cell types of the POP group were enriched in the pathways related to collagen-containing ECM, muscle system processes, neutrophil activation, and other related pathways and were widely downregulated in proteins targeting the endoplasmic reticulum (ER), ribosome biogenesis, and other pathways (Supplementary Fig. A-J). Surprisingly, SMCs downregulated ECM organization pathways (Supplementary Fig. 3C).

# Characterization of stromal cells

Stromal cells are the main cells in the USL, accounting for 73.58% of the cell population. To study the subsets of stromal cells, we conducted a subpopulation analysis of three types of stromal cells (Fig. 2A-F), followed by GO functional enrichment analysis (Supplementary Fig. 4A-C). In addition, pseudo-time analysis was performed on the three types of cells.

Fibroblasts are critical cell components in the USL and play a key role in the ECM. We conducted an unsupervised analysis clustering on 5157 fibroblasts in the sample and divided them into five clusters in the heatmap (Fig. 2A), which were specifically marked as SFRP1 + fibroblasts, FGBP2 + fibroblasts, PCP4 + myofibroblasts, PGS5 + mural cells, and SLPI + fibroblasts (Fig. 2G). Fibroblasts1 with the highest abundance was marked as SFRP1 + fibroblasts, which highly expressed DPT, CCDC80, COL14A1, VEGFD, FBLN1, PI16, and C7 and was identified as universal fibroblasts, which may be the same cell as DPT + PI16 + fibroblasts in the pancreas and human adipose tissue [27]. Fibroblasts2 highly expressed FGBP2, FOXD1, and CYP1B1, defined as FGBP2 + fibroblasts, and was enriched in growth factor binding and mesenchyme development pathways (Supplementary Fig. A). Fibroblasts3 and fibroblasts4 highly expressed muscle contraction-related genes such as ACTA2 and ACTG2. Fibroblasts3 was marked as PCP4 + myofibroblasts. Fibroblasts4 was identified as RGS5 + mural cells by known markers (RGS5, MCAM, NOTCH3, and PDGFRB) [28] (Supplementary Fig. 5) and was enriched in the pathway of oxidative phosphorylation and vascular process in the circulatory system. Fibroblasts5 was marked as SLPI + fibroblasts, which was considered to be a fibroblast related to inflammation, with high expression of WNT10B, MFAP5, SCARA5, and ClEC3B. GO analysis showed SLPI + fibroblasts not only enriched the pathways related to extracellular mechanism but also enriched neutrophil activation and neutrophil degranulation (Supplementary Fig. 4A). Furthermore, we performed a pseudo-time analysis for fibroblast subtypes (Fig. 2J). SFRP1 + fibroblasts and FGBP2 + fibroblasts that regulate the ECM were widely distributed. PCP4 + myofibroblasts and RGS5 + mural cells were mainly distributed at the beginning of the track, and genes related to muscle contraction, such as MYH11 and ACTA2, were highly expressed as well (Fig. 2K). SLPI + fibroblasts were mainly distributed on the right side of the trajectory. In the heatmap of genes that varied in expression over pseudo-time, collagen genes were upregulated at the end of the trajectory (Fig. 2K).

SMCs were the most abundant cells in the USL. A total of 10,377 SMCs were divided into four cell clusters (Fig. 2B). We found that, compared with normal tissues, the proportion of SMCs2 expressed in POP cells increased, whereas the expression of SMCs3 decreased (Fig. 2E). All four clusters highly

expressed stress-related genes, including ATF3, DNAJB1, HSPA1A, HSPA1B, and FOSB (Fig. 2H). SMCs1 is the main cluster expressing stress-related genes. According to its differentially expressed genes, SMCs1 was marked as ATF3 + SMCs. ATF3, FOS, and FOSB, stress related TFs, were identified as key TFs of ATF3 + SMCs (Supplementary Fig. 4D). Additionally, ATF3 + SMCs enriched the regulation of hematopoiesis and the fat cell differentiation pathway (Supplementary Fig. 4B). SMCs2 was marked as CTR9 + SMCs. CTR9 can specifically participate in the regulation of the transcript levels of IL-6 responsive genes by interacting with the JAK/STAT3 pathway [29]. Unfortunately, we did not get any upregulated GO pathway from CTR9 + SMCs. SMCs3 was marked as CFHR1 + SMCs and was enriched in regulation of the immune effector process pathway. Combined with oxidized low-density lipoprotein, CFHR1 can increase the production of inflammatory cytokines by monocytes and neutrophils through activation of pyrin domain-containing protein 3 (NLRP3) [30,31]. Furthermore, CFHR1 + SMCs was enriched in the ECM-associated pathway and may be of the synthetic SMC. The fourth cluster had only 23 cells, which was identified as Schwann cells according to OX2, PLP1, and CD200 (Supplementary Fig. 1). Pseudo-time analysis showed that in the developmental trajectory of SMCs, the SMCs3 cluster was mainly distributed in the early stage, whereas SMCs1 and SMCs2 were mainly distributed in the late stage (Fig. 2L).

Endothelial cells accounted for 21.29% of all the cells. Three subgroups were subdivided into lymphatic endothelial cells (LECs), arterial endothelial cells (AECs), and venous endothelial cells (VECs) (Fig. 2C). The proportion of AECs increased in the POP group (Fig. 2F). We performed GO functional pathway enrichment analysis on endothelial cells (Supplementary Fig. 4C). AECs were enriched in the actin-binding pathway. VECs express proteins targeting the ER pathway. LECs were associated with the collagen-containing ECM and neutrophil activation involved in immune response. Pseudo-time analysis showed that VECs were distributed throughout the track but were expressed more strongly in the early stage, whereas LEC and AEC developed later (Fig. 2N).

# Characterization of myeloid cells

Differences in the type of immune cell infiltration between the POP and control groups were significant. Myeloid cells comprised the largest cell group, except for stromal cells in the USL. There was an increase of macrophages, neutrophils, and mast cells in the POP group than in the control group (Fig. 1D). Four clusters were obtained by unsupervised clustering analysis of macrophages, which highly expressed stress response genes, such as DNAJB1, HSPA1A, HSPA1B, and several cytokine genes, including CXCL2 and CXCL8 (Fig. 3A). According to several simple markers, the macrophages in USL cannot be well classified into proinflammatory M1 and anti-inflammatory M2 categories [32]. M1marker IL1B is mainly distributed in macrophages3 and expressed a part of TNF and NFKB1 (Supplementary Fig. 5) [33,34]; hence, it is considered that macrophages3 may be a M1 subtype. Pathways such as neutrophil activation and leukocyte chemotaxis were enriched in macrophages3. Macrophages1 and macrophages2 has similar characteristics, both of which express a large number of stress-related genes, and neither can be clearly distinguished as M1 or M2 subtype. M1marker CD68, M2marker MRC1, CD163, TGFB1, MERTK, and STAB1 (Supplementary Fig. 5) [35] were distributed in macrophages1 and macrophages2; however, they were more inclined to anti-inflammatory M2 subtype. GO function analysis showed that macrophages1

enriched stress-related pathways, and macrophages2 enriched lipoprotein particle binding and cell-matrix adhesion pathways (Supplementary Fig. A). The fourth cluster had only 22 cells and highly expressed CHIT1, a marker of macrophage activation related to fibrosis [36]. Monocytes were divided into four clusters (Fig. 3B). We found almost all monocytes expressed CD14, and only monocytes3 expressed CD16/FCGR3A (Supplementary Fig. 5). According to this, we suggested monocytes3 were intermediate monocytes (CD14 + CD16+) and the rest were classical monocytes (CD14 + CD16-/low). Intermediate monocytes have different transcription characteristics from other monocytes. Monocytes3 was enriched in the pathway oxidative phosphorylation, RNA catabolic process, and neutrophil activation (Supplementary Fig. 6B), which is consistent with the research of Qian et al. [37]. Monocytes1 highly expressed inflammation-related genes such as IRAK2, CD72, and CCL20 and was enriched in I-kappaB kinase/NF-kappaB signaling, intrinsic apoptotic signaling pathway, and so on. Monocytes2 highly expressed JUN, FOS, and ATF3 transcription factors and early response gene family (EGR2,1,IER2), which were enriched in stress-related pathways. Monocytes4 was mainly enriched in the reaction of metal ions. DCs highly expressed major histocompatibility complex-related genes, which is consistent with the characteristics of DCs as antigen-presenting cells, and were divided into cDC1, cDC2, and matureDC3 (Supplementary Fig. 7A).

In addition, we performed a pseudo-time analysis of the 11 cell clusters of mononuclear phagocytes, and there were 2 branching points in the trajectory (Fig. 3C). The classical monocytes were mainly located in state 1, 2, and 3; intermediate monocytes were located in state 2, 3, and 5; macrophages3 that was possibly a M1 subtype was mainly located in state 4 and 5; and the remaining three macrophage clusters were mainly located in state 4; DCs were located in state 2 and state 5. Pseudo-time analysis showed the development track from classical monocytes to intermediate monocytes, then to macrophages or DC. We further identified genes that varied in expression over pseudo-time. IL1RN, IL1B, and CCL20 were mainly upregulated at the beginning of the pseudo-time, and FOS, JUN, and complement related genes (C1QA, C1QB, and C1QC)were upregulated near the end (Fig. 3D).

The number of neutrophils in the POP group increased significantly, consistent with the results of previous studies [19,20]. Further analysis of 1136 neutrophils in the POP group revealed four clusters with different gene expression profiles (Fig. 3E). Xie et al. mapped neutrophil subpopulations G0–G5 to progressively maturing neutrophils in bone marrow, tissues and circulation[38]. Using the DEGs provided by Xie et al., we conducted correlation analysis (Fig. 3F), and found that Neutrophils1 were similar with G3-5a, Neutrophils2 were similar with G2, G5a and G5c, and neutrophils3 and G5b were the same subpopulations. Correlation analysis showed Neutrophils4 were different from any subpopulation of G0-G5. However, according to the known neutrophil typing markers provided by Chen + et al [39], we suggested that Neutrophils4 were G5c (Fig. 3G). Neutrophils1 had the characteristics of G3-5a which were relatively immature neutrophils compared with G5b and G5c, and highly expressed gelatinase granule gene MMP9, and enriching neutrophil degranulation/neutrophil activation pathway. Neutrophils3 expressed a large number of interferon-induced proteins (RSAD2, IFIT1, IFIT3, HERC5, MX1) and were enriched in interferon-related pathways (Supplementary Fig. 7B). These characteristics were consistent with G5b in tissues and

umbilical cord blood. Neutrophils2 secreted a large number of cytokines, such as IL1B, CCL4L2, CCL4, IL1A, IL1RN, CXCL1, and CXCL2, and enriched in response to lipopolysaccharide and cellular response to interleukin-1 pathway. Neutrophils4 only has 47 DEGs, indicating the similarity between neutrophils4 and other subpopulations.

Mast cells highly expressed TPSAB1, TPSB2, and CPA3. GO analysis showed that the upregulated pathways in mast cells were related to immune cell activation, while significantly downregulated ECM and other pathways.The number of lymphocytes was relatively small, and the number of T cells was significantly higher in the POP group than in the control group (Fig. 1D). Cluster analysis of T cells revealed naïve T cells, CD8 effector T cells, and NKT cells (Supplementary Fig. 7C).

# Cell-Cell interaction patterns in POP and control samples

We performed cell–cell interaction analysis using CellphoneDB in the USL. In all groups, an intensive interaction between fibroblasts and endothelial cells was observed in stromal cells (Fig. 4A). In immune cells, we observed a dense communication network among neutrophils, macrophages, DCs, and monocytes, suggesting the importance of these cell–cell interactions in the USL (Fig. 4A). In addition, we identified receptor–ligand pairs in the control and POP groups respectively. Cell–cell interactions in the POP group were attenuated compared with those in the control group (Fig. 4B).

We assessed the specific interactions between endothelial cells and fibroblasts (Fig. 4C). In the control group, fibroblasts secreted a large number of collagen-like genes such as MMP2, FN1, LAMC1, and OMD to interact with endothelial cells. In addition, EPHB4_EFNB1, FLT1 complex_PGF, VEGFA_FLT1, and VEGFD_KDR receptor–ligand pairs promoted endothelial cell growth. FLT1 and KDR encode members of the vascular endothelial growth factor receptor (VEGFR) family and play critical roles in angiogenesis and vasculogenesis [40]. Endothelial cells and fibroblasts promote fibroblast growth and development through FGFR1_FGF7 and FGFR1_NCAM1 receptor–ligand pairs. Above, we reported that the proportion of ECs was reduced in the POP group compared with that in the control group. Accordingly, the interaction between ECs and fibroblasts was further significantly reduced in the POP group (Fig. 4B), which was mainly reflected by the significant reduction in receptor–ligand pairs related to ECM and cell adhesion. However, there was no significant difference in VEGF or FGF levels, and a large number of growth factor interaction pairs were still enriched in the POP group.

Compared with the control group, neutrophils increased significantly in the USL of the POP group (Fig. 1D), and there was a rich cellular communication network between neutrophils and mononuclear phagocytes. We found that, in the POP group, mononuclear phagocytes secreted large amounts of CXCL3 and CXCL8, which were bound to CXCR1 and CXCR2 in neutrophils, thus attracting neutrophils to the USL site (Fig. 4D). Several interleukin-1 (IL-1) family gene interactions were detected between neutrophils and other immune cells. In particular, IL-1B was most active in monocytes (Fig. 4E). ICAM1, ICAM2, and ICAM3 in neutrophils and MPs played a role in cell adhesion and regulating inflammation. These four cell types regulate the extracellular matrix through HGF_CD44 and CD44_HBEGF receptor-ligand pairs and then regulate cell adhesion and migration (Fig. 4E). The CD74_MIF receptor–ligand pair was highly

expressed in immune cells other than neutrophils, and EGFR_MIF, EGFR, and several growth factor receptor–ligand pairs are expressed in fibroblasts interacting with other cells (Fig. 4F). Among them, TGFB1 had been proven to attenuate the loss of ECM by inhibiting the activities of MMP-2/9 through the TGF-β1/Smad3 signaling pathway in USL, and was inversely correlated with the severity of POP [41]. In addition, we found several classes of chemokines, cytokines, and growth factors that were highly expressed (Supplementary Fig. 8A-C).

# Transcriptional regulation in POP and control samples

Combinatorial interactions between TFs lead to tissue-specific gene expression, which determines cell identity and maintains cell homeostasis. We used Transcription factor regulatory network analysis (SCENIC )to assess the expression of TFs in the USL and to identify key TFs. First, we investigated the expression of TFs and cell-type-specific TFs in the control group. Highly expressed NFATC2 in macrophages, neutrophils and monocytes, GATA3 in mast cells and T cells, and STAT4 in T cells can all promote T-cell differentiation (Fig. 5A, Supplementary Fig. 9). High basal expression of STAT4 contributes to the NKT cell responses [42]. GO functional enrichment analysis was performed on these TFs, and MYBL2, GATA3, and ARID3A were enriched in lymphocyte differentiation and regulation of myeloid leukocyte differentiation (Fig. 5B).

Furthermore, we investigated the TFs in the POP group. The specific TFs in neutrophils were the same as those in the control group; however, the expression intensity was significantly enhanced (Fig. 5A-B, Supplementary Fig. 9). In addition to neutrophils, we observed that, except for the TFs already highly expressed in the control group, another group of TFs was specifically highly expressed in the POP group. Several specific TFs of monocyte, such as OLIG1, CEBPE, POU2F2, and NFE2, were all enriched in neutrophil activation (Fig. 5C-D). C/EBP family is related to neutrophil proliferation, differentiation, maturation, and granular protein formation [43]. CEBPE and NFE2 were specific TFs of neutrophils. CEBPE could promote the terminal differentiation of neutrophils [44]. E2f2 contributed to neutrophil commitment [38]. NFE2L3 was specifically active in mast cells and was enriched in ECM organization, suggesting that the increase in mast cells in POP samples is critical for the development of ECM remodeling and prolapse.

In addition, TFs of stromal cell in the control and POP groups tended to be functionally similar, and both were related to the development, differentiation, and proliferation of specific cells. However, the TF function of the stromal cells in the POP group was more closely related to cell function. Fibroblast-specific TFs, such as PBX1, ARRM3, and AR, were significantly upregulated, all of which are related to ECM remodeling. The SMC-specific TFs FOXC2, TBX2, EMX2, and ISL1 play important roles in muscle development. ZNF233, SP6, and SMAD1 were highly active in endothelial cells and contribute to vascular development t (Fig. 5A-D). These potential upstream regulators contribute to our understanding of the pathogenesis of POP.

# Discussion

POP markedly affects the health and quality of life of women, and there is no optimal treatment. The uterosacral ligament, which provides apical support for the upper part of the uterus and vagina, plays an integral role in POP. Although POP has been extensively studied, its key mechanisms have not been fully elucidated; in particular, the role of immune cells, including macrophages, monocytes, DCs, and neutrophils, in POP pathology is unclear. For the first time, we performed a scRNA-seq analysis using samples from the USL in POP patients and control patients to elucidate the cellular composition of the USL and the expression of specific genes for its different cell types and to provide a better understanding of the pathophysiological mechanisms and the immune microenvironment of POP. We identified 10 cell types, including 3 stromal and 7 immune cells. We performed unsupervised graph clustering, GO functional enrichment analysis, and TF analysis on these cells, and pseudo-time analysis of some cells, which revealed heterogeneity between the main mesenchymal cells and immune cells. In addition, we found alterations in cell–cell interactions and TFs in POP. Overall, our study greatly deepens our understanding of the pathological mechanisms of POP and provides a theoretical basis for the development of related therapeutic strategies.

Previous studies have suggested that the main component of USL is the ECM; however, we still found a large number of cell types in USL. Fibroblasts, SMC, and endothelial were the main cell types of USL, accounting for 17.36%, 34.93%, and 21.29%, respectively. We verified the universal phenotype and differentiation of fibroblasts proposed by Buechler et al [27]. DEGs analysis showed that SFRP1 + fibroblasts, which was widely present in the USL, highly expressed the upregulated genes such as DPT, C7, MFAP4, and LUM, of universal fibroblasts. The trajectory of fibroblast subtypes indicated that universal fibroblasts differentiated into specialized fibroblasts (SLPI + fibroblasts) during development. In addition to enriched functions such as the organization of the ECM and muscle system process, clustering analysis revealed that the subgroups SLPI + fibroblasts, ATF3 + SMCs, and LEC were enriched in neutrophil activation, immune response, and neutrophil degranulation, respectively. Immune cells differed markedly between the POP and control samples. Compared to the control group, neutrophils, macrophages, mast cells, and T cells increased significantly in the POP group. Based on several clusters enriched in pathway neutrophils activation, we did find that neutrophils increased significantly at the same time. We divided neutrophils into four clusters and found that these four clusters can correspond to the neutrophils in Chen and Xie et al.'s single cell RNA sequencing studies [38,39], which further verified the phenotype of neutrophils in the human body. In addition, according to a widely used previous classification scheme, macrophages were grouped into pro-inflammatory (M1) and an anti-inflammatory (M2) phenotypes. However, several markers cannot separate macrophages well. Some macrophage clusters expressed both M1 and M2 markers. According to the distribution of M1 and M2 markers, we found that macrophages3 had the characteristics of M1, and the remaining cell population had the characteristics of M2; however, it cannot be strictly considered as M1/M2 phenotype.

In addition, we found that smooth muscle cells and macrophages in the uterosacral ligament showed strong expression of stress-response genes [45]. SMCs3-specific marker CFHR1 can bind to necrotic oxidized low-density lipoprotein and strongly induces inflammasome NLRP3 in monocytes and

neutrophils by exposure to EMR2 and then secretes pro-inflammatory cytokines such as IL-1β, IL-6.IL18, and TNFα [30,31]. In this study, the expression of EMR2/ADGRE2 was observed in macrophages, and the high expression of NLRP3 was observed in monocytes1 and neutrophils 2. Furthermore, cell–cell interaction analysis found that many IL-1 interactions happened between neutrophils with other cells. This may be a point in the pathogenesis of POP stress.

After sequencing the USL samples, we identified a high percentage of endothelial cells in all USL samples. Compared with the control sample, there was a significantly lower percentage of endothelial cells in the POP samples. At the same time, endothelial cells and fibroblasts showed active cell–cell interactions in the control group but were less active in the POP group. This change was reflected mainly by the high expression of ECM-related interaction pairs between fibroblasts and endothelial cells in the control group, which was significantly reduced in the POP group. In addition, we predicted that there was a symbiotic relationship between fibroblasts and endothelial cells in a two-cell circuit in both the control and POP groups and that they interacted mutually to obtain growth factor signals. Endothelial cells promote fibroblast development by providing FGFR1, whereas fibroblasts promote proliferation, migration, and differentiation of ECs by supplying VEGF and VEGFD. Furthermore, monocytes and macrophages recruit neutrophils through the interaction of CXCL3 and CXCL8 with CXCR1 and CXCR2. Neutrophils express many IL-1 family genes that have been shown to play a key role in inflammation, fibrosis, and autoimmune reactions [46,47]. Therefore, IL-1 family interaction may be a reason for promoting collagen deposition in the POP sacral ligament. In addition, we found that CD74_MIF receptor-ligand pairs are widely expressed in immune cell interactions and may activate the expression of factors related to proliferation and fibrosis of fibroblasts, such as EGFR and TGFB1 [48–50]. That is, MIF-CD74 may be a crucial receptor–ligand pair linking immune and extracellular remodeling mechanisms in POP. In conclusion, we have identified several critical receptor–ligand pairs for fibroblast–immune cell interactions.

TFs activate or repress gene transcription by recruiting other TFs, coactivators, or corepressors to affect the cell state. We found that FOS and JUN were significantly overexpressed in monocytes2 and mast cells and that JUNB was highly expressed in macrophages1 and monocytes2. These TFs may increase the inflammatory responses of macrophages, monocytes, and mast cells. Furthermore, we identified a series of TFs related to cell development and proliferation, including EOMES, NFE2, PBX1, SOX7, and TBX2. In addition, we found that TFs related to neutrophil activation were specifically active on monocytes in POP samples. Moreover, GO functional pathway analysis of differentially expressed genes in monocytes was enriched in the neutrophil activation-related pathways, indicating that monocytes may be a key cell type regulating neutrophil activity. Furthermore, we found a critical upstream TF, NFE2L3, which was enriched in ECM-related pathways in mast cells. Simultaneously, GO analysis showed that mast cells were significantly downregulated in pathways such as ECM organization, indicating that mast cells may play crucial roles in the regulation of ECM in the USL. Collectively, we propose that the ECM interacts with the immune system, possibly causing the accumulation and remodeling of the ECM, and

the accumulation of ECM leads to the proliferation of immune cells, leading to a sustained inflammatory response [51,52].

In this study, we integrated scRNA-seq datasets from three POP samples and one hysteromyoma control sample. Since we needed sufficiently large USL tissue from resected uterine specimens in patients who underwent total hysterectomy for benign reasons, we had insufficient samples for the control group. The sample size of the control group was smaller than that of the POP group, which may have limited the statistical power of this comparison. Furthermore, the ethnic and racial matching of the POP and control groups was poor. All patients were of Han nationality. Additional control specimens from different sources should be evaluated in future studies to address these limitations. Furthermore, because adipocytes are very light, scRNA-seq technology cannot obtain information on adipocytes, which may lead to the loss of adipocyte composition and heterogeneity in the USL. Single-cell nuclear RNA sequencing technology is required to provide further elucidation. Finally, this study lacked verification tests to prove the relevant mechanisms mentioned in this paper. More verification tests are needed to prove potential pathogenesis in the future.

Our study was the first to explore the cell type composition and heterogeneity of POP and normal USLs, revealing a picture of immune cell infiltration in USL tissue of POP samples. We had verified some previous cell clusters of human fibroblasts and neutrophils and found new clusters of uterosacral ligaments. In addition, we found that fibroblasts and endothelial cells promoted the growth, proliferation, and development of each other and described how immune cells and fibroblasts communicate with each other through receptor-ligand pairs. Furthermore, we identified important TFs that regulate the ECM, cell development, and immune response. Overall, our study con-tributes to improving our understanding of the pathogenesis of POP and provides relevant information for future research directions and disease prevention strategies.

# Methods

# Sample collection and processing

This study was approved by the Ethics Committee of Shanxi Bethune Hospital (YXLL-2022-131). All participants provided written informed consent to provide samples. This study included women who underwent hysterectomy for POP and hysteromyoma. Patients with Pelvic Organ Prolapse Quantification (POP-Q) stage III–IV were enrolled in the study following the diagnosis by the same experienced specialist. Women who underwent hysterectomy for hysteromyoma and did not have prolapse were included as the control group. Exclusion criteria were previous pelvic reconstruction surgery, chronic pelvic inflammation, autoimmune diseases, connective tissue diseases, and malignant tumors. All patients were non-smokers, aged > 40 years, and had a BMI ranging 18.5–28 $kg/m^2$. Approximately 1–1.5 $cm^3$ of the cervical attachment of the USL was collected from the hysterectomy specimen of the patient and was used for the preparation of the single-cell suspension in the next step.

# Tissue dissociation and preparation

The fresh tissues were stored in the sCelLiveTM Tissue Preservation Solution (Singleron Bio Com, Nanjing, China) on ice after the surgery within 30 mins. The specimens were washed with Hanks Balanced Salt Solution (HBSS) for 3 times and then digested with 2 ml sCelLiveTM Tissue Dissociation Solution (Singleron) by Singleron PythoN™ Automated Tissue Dissociation System (Singleron) at 37°C for 15 mins. Afterwards, the GEXSCOPE® red blood cell lysis buffer (Singleron, 2ml) was added, and cells were incubated at 25°C for another 10 mins to remove red blood cells. The solution was then centrifuged at 500×g for 5 mins and suspended softly with PBS. Finally, the samples were stained with trypan blue (Sigma, United States) and the cellular viability was evaluated microscopically.

# Library preparation and scRNA-seq

Single-cell suspensions (1×105 cells/ml) with PBS (HyClone) were loaded into microfluidic devices using the Singleron Matrix® Single Cell Processing System (Singleron). Subsequently, the scRNA-seq libraries were constructed according to the protocol of the GEXSCOPE® Single Cell RNA Library Kits (Singleron) [53]. Individual libraries were diluted to 4 nM and pooled for sequencing. At last, pools were sequenced on Illumina novaseq6000 with 150 bp paired end reads.

# Quality control, dimension-reduction and clustering (Scanpy)

Scanpy v1.8.2 was used for quality control, dimensionality reduction and clustering under Python 3.7 [54]. For each sample dataset, we filtered expression matrix by the following criteria: 1) cells with gene count less than 200 or with top 2% gene count were excluded; 2) cells with top 2% UMI count were excluded; 3) cells with mitochondrial content > 30% were excluded; 4) genes expressed in less than 5 cells were excluded. After filtering, 30452 cells were retained for the downstream analyses, with on average 1424 genes and 4562 UMIs per cell. The raw count matrix was normalized by total counts per cell and logarithmically transformed into normalized data matrix. Top 2000 variable genes were selected by setting flavor = 'seurat'. Batch effect between samples was removed by Harnomy. Cells were separated into 23 clusters by using Louvain algorithm and setting resolution parameter at 1.2. Cell clusters were visualized by using Uniform Manifold Approximation and Projection (UMAP).

# Differentially expressed genes analysis

Genes expressed in more than 10% of the cells in a cluster and with average log (Fold Change) of greater than 0.25 were selected as DEGs by Seurat v3.1.2 FindMarkers based on Wilcox likelihood-ratio test with default parameters.

# Cell type annotation

The cell type identity of each cluster was determined with the expression of canonical markers found in the DEGs using SynEcoSys database. Heatmaps/dot plots/violin plots displaying the expression of markers used to identify each cell type were generated by Scanpy v1.8.2. Cell doublets were estimated

based on the expression pattern of canonical cell markers. Any clusters enriched with multiple cell type-specific markers were excluded for downstream analysis.

# Pathway enrichment analysis

To investigate the potential functions of all cell types, Gene Ontology (GO) analysis were used with the "clusterProfiler" R package 3.16.1 [55]. Pathways with p_adj value less than 0.05 were considered as significantly enriched. Gene Ontology gene sets including molecular function (MF), biological process (BP), and cellular component (CC) categories were used as reference.

# Trajectory analysis

To map differentiation/conversion of cell subtypes in fibroblsts, SMC, EC, and myeoid cells, pseudo-time trajectory analysis was performed with Monocle2 [55–57]. The trajectory was visualized by plot_cell_trajectory.

# Cell-cell interaction analysis (CellPhoneDB)

Cell-cell interaction (CCI) were predicted based on known ligand–receptor pairs by Cellphone DB v2.1.0 [58]. Permutation number for calculating the null distribution of average ligand-receptor pair expression in randomized cell identities was set to 1000. Individual ligand or receptor expression was thresholded by a cutoff based on the average log gene expression distribution for all genes across each cell type. Predicted interaction pairs with p value < 0.05 and of average log expression > 0.1 were considered as significant.

# Transcription factor regulatory network analysis (scenic)

Transcription factor network was constructed by single-cell regulatory network inference and clustering (SCENIC) R toolkit (ref) using scRNA expression matrix and transcription factors in AnimalTFDB [59]. The GENIE3 package predicted a regulatory network based on the co-expression of regulators and targets. RcisTarget package searched for transcription factor binding motifs in the given data. Genes involved in the predicted regulatory network were defined as a gene set, and AUCell package calculated the auc value of the gene set to assess the activity of regulatory network in cells.

# Differential proportion analysis.

Differential proportion analysis was performed based on the ratio change. Firstly, we got the proportion of each cell type or subtype by dividing the numbers of cells by the total number of cells. Then, the Log2-fold change was calculated between POP and control samples and |Log2-fold change | > 0.5 was considered as threshold for significant change.

# Statistics and reproducibility

We performed scRNA sequencing of the USL in three patients with POP and one control patient who had undergone hysterectomy for hysteromyoma.

# Declarations

### Data availability

We are uploading our scRNA-seq data to Gene Expression Omnibus. When this study is confirmed to be published in this journal, the dataset of this study will be uploaded to Gene Expression Omnibus.


### Acknowledgments

We are grateful to Singleron team for the continuous support. We would like to thank Editage (www.editage.cn) for English language editing.


### Author contributions

MS and JZ designed and performed experiments, analyzed the data, and wrote the paper. LW and XilingL analyzed the data. XiaoL, WW and QH provided human samples. XiaoL initiated and designed the study. All authors contributed to the article and approved the submitted version.

### Competing interests

The authors declare that the research was conducted in the absence of any commercial or financial relationships that could be construed as a potential conflict of interest.

# References


1. Weintraub, A. Y., Glinter, H. & Marcus-Braun, N., Narrative review of the epidemiology, diagnosis and pathophysiology of pelvic organ prolapse. *INT BRAZ J UROL* **46** 5 (2020).
2. Barber, M. D., Pelvic organ prolapse. *BMJ* **354** i3853 (2016).
3. Barber, M. D. & Maher, C., Epidemiology and outcome assessment of pelvic organ prolapse. *INT UROGYNECOL J* **24** 1783 (2013).
4. Walker, G. J. & Gunasekera, P., Pelvic organ prolapse and incontinence in developing countries: review of prevalence and risk factors. *INT UROGYNECOL J* **22** 127 (2011).
5. Li, Z. Y. *et al.*, An epidemiologic study of pelvic organ prolapse in urban Chinese women: a population-based sample in China. *Zhong hua yi xue za zhi* **99** 857 (2019).
6. Wu, J. M. *et al.*, Prevalence and trends of symptomatic pelvic floor disorders in U.S. women. *OBSTET GYNECOL* **123** 141 (2014).
7. Wu, J. M., Hundley, A. F., Fulton, R. G. & Myers, E. R., Forecasting the prevalence of pelvic floor disorders in U.S. Women: 2010 to 2050. *OBSTET GYNECOL* **114** 1278 (2009).
8. Olsen, A. L., Smith, V. J., Bergstrom, J. O., Colling, J. C. & Clark, A. L., Epidemiology of surgically managed pelvic organ prolapse and urinary incontinence. *OBSTET GYNECOL* **89** 501 (1997).

9. Cattani, L. *et al.*, Pregnancy, labour and delivery as risk factors for pelvic organ prolapse: a systematic review. *INT UROGYNECOL J* **32** 1623 (2021).
10. Vergeldt, T. F., Weemhoff, M., IntHout, J. & Kluivers, K. B., Risk factors for pelvic organ prolapse and its recurrence: a systematic review. *INT UROGYNECOL J* **26** 1559 (2015).
11. Ramanah, R., Berger, M. B., Parratte, B. M. & DeLancey, J. O., Anatomy and histology of apical support: a literature review concerning cardinal and uterosacral ligaments. *INT UROGYNECOL J* **23** 1483 (2012).
12. Tan, T. *et al.*, Histo-mechanical properties of the swine cardinal and uterosacral ligaments. *J Mech Behav Biomed Mater* **42** 129 (2015).
13. CAMPBELL, R. M., The anatomy and histology of the sacrouterine ligaments. *AM J OBSTET GYNECOL* **59** 1 (1950).
14. Lim, V. F., Khoo, J. K., Wong, V. & Moore, K. H., Recent studies of genetic dysfunction in pelvic organ prolapse: the role of collagen defects. *Aust N Z J Obstet Gynaecol* **54** 198 (2014).
15. Zeng, C. *et al.*, Correlation Between Autophagy and Collagen Deposition in Patients With Pelvic Organ Prolapse. *Female Pelvic Med Reconstr Surg* **24** 213 (2018).
16. Guler, Z. & Roovers, J. P., Role of Fibroblasts and Myofibroblasts on the Pathogenesis and Treatment of Pelvic Organ Prolapse. *Biomolecules* **12** (2022).
17. Mei, S. *et al.*, The role of smooth muscle cells in the pathophysiology of pelvic organ prolapse. *Female Pelvic Med Reconstr Surg* **19** 254 (2013).
18. Khadzhieva, M. B., Kolobkov, D. S., Kamoeva, S. V. & Salnikova, L. E., Expression changes in pelvic organ prolapse: a systematic review and in silico study. *Sci Rep* **7** 7668 (2017).
19. Zhao, Y., Xia, Z., Lin, T. & Yin, Y., Significance of hub genes and immune cell infiltration identified by bioinformatics analysis in pelvic organ prolapse. *PEERJ* **8** e9773 (2020).
20. Orlicky, D. J. *et al.*, Using the novel pelvic organ prolapse histologic quantification system to identify phenotypes in uterosacral ligaments in women with pelvic organ prolapse. *AM J OBSTET GYNECOL* **224** 61 (2021).
21. Li, Y. *et al.*, Single-cell transcriptome profiling of the vaginal wall in women with severe anterior vaginal prolapse. *NAT COMMUN* **12** 87 (2021).
22. Liu, C. *et al.*, Collagen metabolic disorder induced by oxidative stress in human uterosacral ligamentderived fibroblasts: A possible pathophysiological mechanism in pelvic organ prolapse. *MOL MED REP* **13** 2999 (2016).
23. Ward, R. M. *et al.*, Genetic epidemiology of pelvic organ prolapse: a systematic review. *AM J OBSTET GYNECOL* **211** 326 (2014).
24. Zhang, L. *et al.*, Molecular mechanism of extracellular matrix disorder in pelvic organ prolapses. *MOL MED REP* **22** 4611 (2020).
25. Ak, H. *et al.*, Microarray gene expression analysis of uterosacral ligaments in uterine prolapse. *CLIN BIOCHEM* **49** 1238 (2016).

26. Zhou, Q., Hong, L. & Wang, J., Identification of key genes and pathways in pelvic organ prolapse based on gene expression profiling by bioinformatics analysis. *ARCH GYNECOL OBSTET* **297** 1323 (2018).
27. Buechler, M. B. *et al.*, Cross-tissue organization of the fibroblast lineage. *NATURE* **593** 575 (2021).
28. Muhl, L. *et al.*, Single-cell analysis uncovers fibroblast heterogeneity and criteria for fibroblast and mural cell identification and discrimination. *NAT COMMUN* **11** (2020).
29. Youn, M. *et al.*, hCTR9, a Component of Paf1 Complex, Participates in the Transcription of Interleukin 6-responsive Genes through Regulation of STAT3-DNA Interactions. *J BIOL CHEM* **282** 34727 (2007).
30. Irmscher, S. *et al.*, Serum FHR1 binding to necrotic-type cells activates monocytic inflammasome and marks necrotic sites in vasculopathies. *NAT COMMUN* **10** (2019).
31. Irmscher, S. *et al.*, Factor H-related protein 1 (FHR-1) is associated with atherosclerotic cardiovascular disease. *SCI REP-UK* **11** (2021).
32. Murray, P. J. *et al.*, Macrophage activation and polarization: nomenclature and experimental guidelines. *IMMUNITY* **41** 14 (2014).
33. Li, Y. *et al.*, Single-Cell Transcriptome Analysis Reveals Dynamic Cell Populations and Differential Gene Expression Patterns in Control and Aneurysmal Human Aortic Tissue. *CIRCULATION* **142** 1374 (2020).
34. Ishikawa, S. *et al.*, Apoptosis inhibitor of macrophage depletion decreased M1 macrophage accumulation and the incidence of cardiac rupture after myocardial infarction in mice. *PLOS ONE* **12** e187894 (2017).
35. Cheng, J. *et al.*, Single-cell RNA sequencing reveals cell type- and artery type-specific vascular remodelling in male spontaneously hypertensive rats. *CARDIOVASC RES* **117** 1202 (2021).
36. Rosa, M. *et al.*, Modulation of Chitotriosidase During Macrophage Differentiation. *CELL BIOCHEM BIOPHYS* **66** 239 (2013).
37. Qian, J. *et al.*, Single-Cell RNA Sequencing of Peripheral Blood Mononuclear Cells From Acute Myocardial Infarction. *FRONT IMMUNOL* **13** (2022).
38. Xie, X. *et al.*, Single-cell transcriptome profiling reveals neutrophil heterogeneity in homeostasis and infection. *NAT IMMUNOL* **21** 1119 (2020).
39. Chen, Y. *et al.*, Primitive genotypic characteristics in umbilical cord neutrophils identified by single-cell transcriptome profiling and functional prediction. *FRONT IMMUNOL* **13** (2022).
40. Sato, Y. *et al.*, Properties of two VEGF receptors, Flt-1 and KDR, in signal transduction. *Ann N Y Acad Sci* **902** 201, 205 (2000).
41. Liu, C. *et al.*, Role of transforming growth factor beta-1 in the pathogenesis of pelvic organ prolapse: A potential therapeutic target. *INT J MOL MED* **40** 347 (2017).
42. Suarez-Ramirez, J. E., Tarrio, M. L., Kim, K., Demers, D. A. & Biron, C. A., CD8 T cells in innate immune responses: using STAT4-dependent but antigen-independent pathways to gamma interferon during viral infection. *MBIO* **5** e1914 (2014).

43. Zhang, D. E. *et al.*, Function of PU.1 (Spi-1), C/EBP, and AML1 in early myelopoiesis: regulation of multiple myeloid CSF receptor promoters. *Curr Top Microbiol Immunol* **211** 137 (1996).
44. Evrard, M. *et al.*, Developmental Analysis of Bone Marrow Neutrophils Reveals Populations Specialized in Expansion, Trafficking, and Effector Functions. *IMMUNITY* **48** 364 (2018).
45. Habes, D., Kestranek, J., Stranik, J., Kacerovsky, M. & Spacek, J., Is there an association between pelvic organ prolapse and oxidative stress? A systematic review. *PLOS ONE* **17** e271467 (2022).
46. Borthwick, L. A., The IL-1 cytokine family and its role in inflammation and fibrosis in the lung. *SEMIN IMMUNOPATHOL* **38** 517 (2016).
47. Maculewicz, E. *et al.*, The interactions between interleukin-1 family genes: IL1A, IL1B, IL1RN, and obesity parameters. *BMC GENOMICS* **23** 112 (2022).
48. Akin, M. N., Sivaslioglu, A. A., Edgunlu, T., Kasap, B. & Celik, S. K., SMAD2, SMAD3 and TGF-beta GENE expressions in women suffering from urge urinary incontinence and pelvic organ prolapse. *MOL BIOL REP* **48** 1401 (2021).
49. Zhang, Y. *et al.*, Macrophage migration inhibitory factor regulates joint capsule fibrosis by promoting TGF-beta1 production in fibroblasts. *INT J BIOL SCI* **17** 1837 (2021).
50. Marcu, R. D. *et al.*, Oxidative Stress: A Possible Trigger for Pelvic Organ Prolapse. *J IMMUNOL RES* **2020** 1 (2020).
51. Jurgensen, H. J. *et al.*, Cellular uptake of collagens and implications for immune cell regulation in disease. *CELL MOL LIFE SCI* **77** 3161 (2020).
52. Wu, C. *et al.*, Bioinformatically deciphering immune cell infiltration and signature genes in pelvic organ prolapse. *INT UROGYNECOL J* (2022).
53. Dura, B. *et al.*, scFTD-seq: freeze-thaw lysis based, portable approach toward highly distributed single-cell 3' mRNA profiling. (2019).
54. Wolf, F. A., Angerer, P. & Theis, F. J., SCANPY: large-scale single-cell gene expression data analysis. *GENOME BIOL* **19** 15 (2018).
55. Yu, G., Wang, L. G., Han, Y. & He, Q. Y., clusterProfiler: an R package for comparing biological themes among gene clusters. *OMICS* **16** 284 (2012).
56. Hanzelmann, S., Castelo, R. & Guinney, J., GSVA: gene set variation analysis for microarray and RNA-seq data. *BMC BIOINFORMATICS* **14** 7 (2013).
57. Qiu, X. *et al.*, Single-cell mRNA quantification and differential analysis with Census. *NAT METHODS* **14** 309 (2017).
58. Efremova, M., Vento-Tormo, M., Teichmann, S. A. & Vento-Tormo, R., CellPhoneDB: inferring cell-cell communication from combined expression of multi-subunit ligand-receptor complexes. *NAT PROTOC* **15** 1484 (2020).
59. Aibar, S. *et al.*, SCENIC: single-cell regulatory network inference and clustering. *NAT METHODS* **14** 1083 (2017).

# Figures

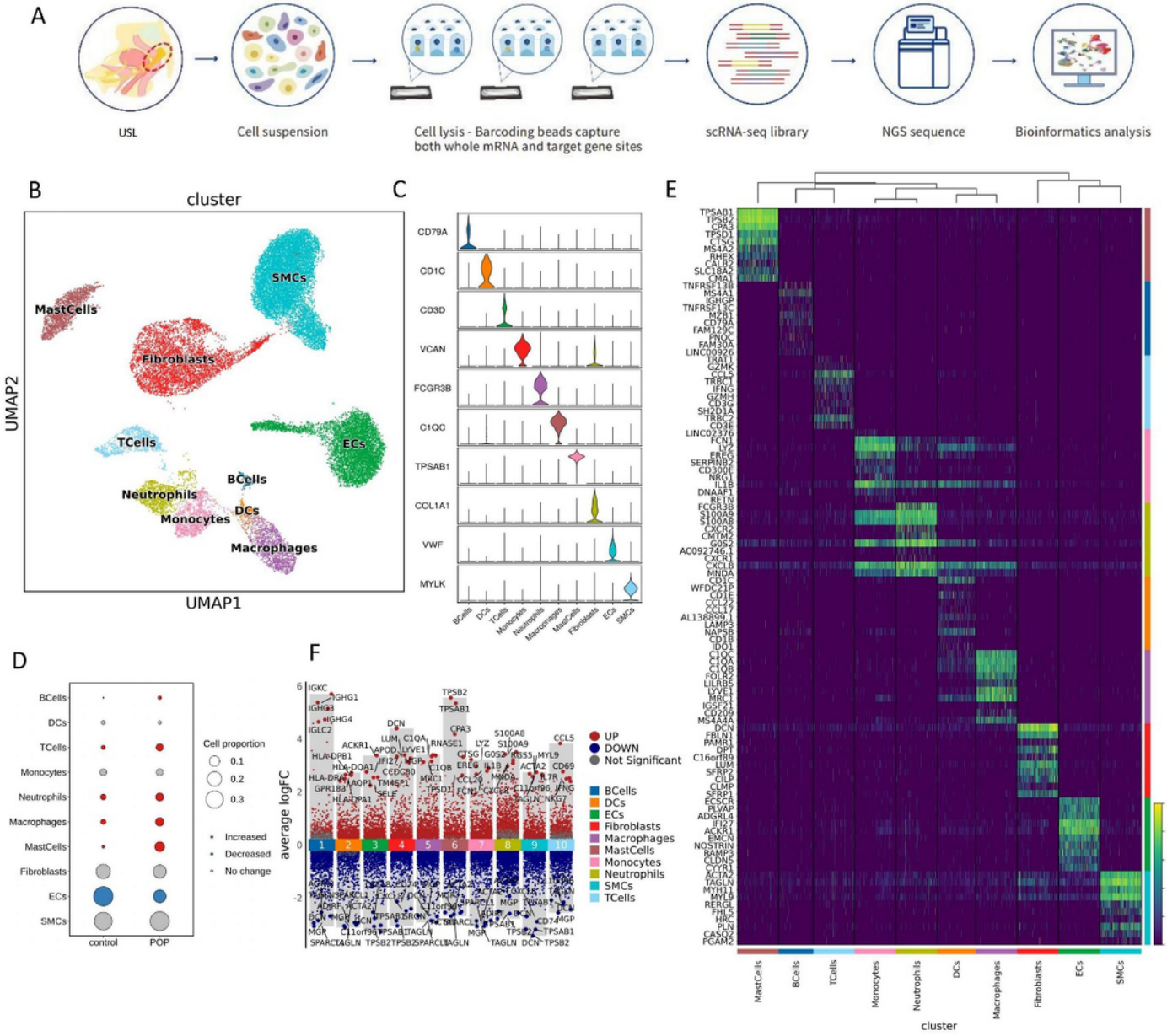


## Figure 1

Diverse cell clusters in the uterosacral ligament with Single-cell RNA-seq analysis.

(A) Schematic representation showing tissue dissociation, cell suspension, cell lysis, library building, sequencing and bioinformatics analysis.

(B) UMAP plots of the 30,452 cells illustrating ten subpolpulations.

(C) Violin plots showing the expression of one canonical marker for each cell type.

(D) Heatmap showing the relative expression of top 10 genes in each cell type.

(E) Comparison of the ratio of cells in POP and control samples.

(F) Volcano plot showing the differentially expressed genes of POP compared with control sample. SMC smooth muscle cells, EC endothelial cells, DCs dendritic cells.

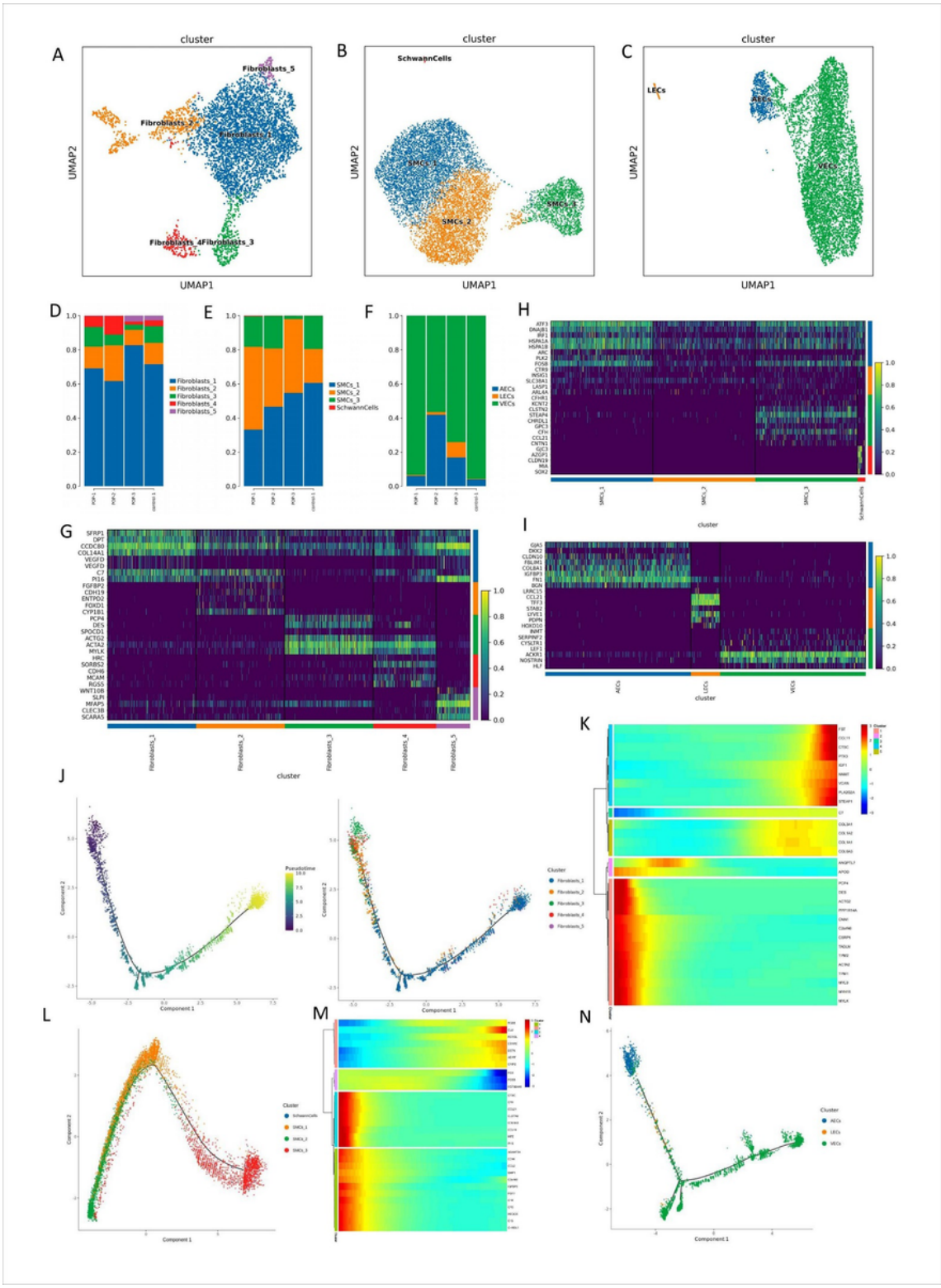


**Figure 2**

Subclustering of fibroblasts, SMCs and DCs in USL reveals cellular heterogeneity

(A-C) UMAP plots showing the subclusters of fibroblasts, SMCs and ECs subtypes in turn.

(D-F) Bar plots showing the percentage of the subclusters of fibroblasts, SMCs and ECs in control and POP samples in turn.

(G) Heatmap showing the differentially expressed genes of five fibroblast subclusters.

(H) Heatmap showing the differentially expressed genes of four smooth muscle cells subclusters.

(I) Heatmap showing the differentially expressed genes of three endothelial cells subclusters.

(J) Trajectory reconstruction of all single cells of five fibroblast subclusters and the distribution of five fibroblast subclusters on the trajectory are shown.

(K) Heatmap showing the dynamic changes of gene expression with pseudo-time in fibroblasts.

(L) The distribution of four subclusters of smooth muscle cell on the trajectory are shown.

(M) Heatmap showing the dynamic changes of gene expression with pseudo-time in SMCs.

(N) The distribution of three subclusters of endothelial cells on the trajectory are shown.

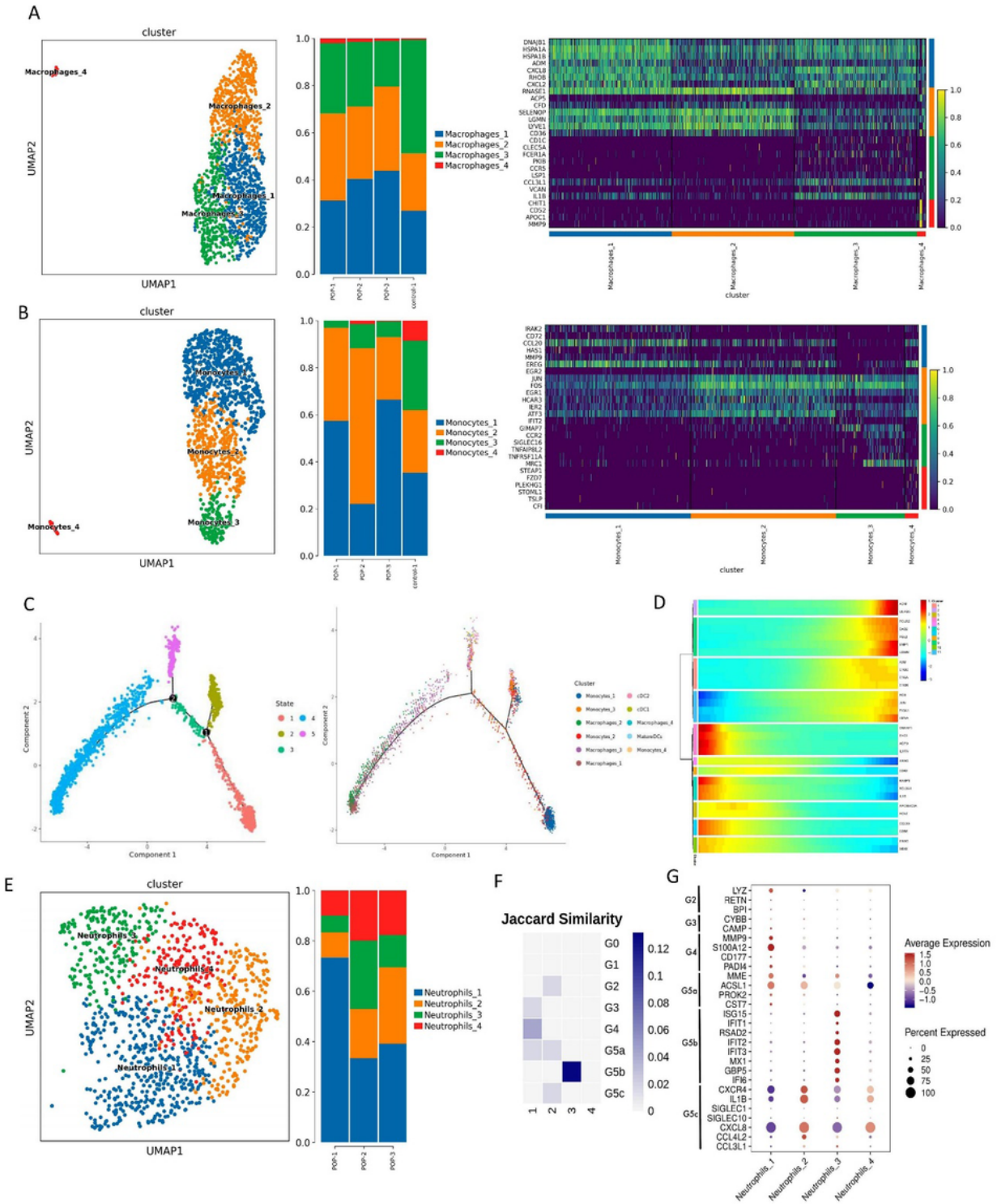


## Figure 3

Subclustering of immune cells in USL reveals cellular heterogeneity

(A)UMAP plot showing the subclusters of macrophages. Bar plot showing the percentage and heatmap showing the differentially expressed genes of four macrophage subclusters.

(B)UMAP plot showing the subclusters of monocytes. Bar plots showing the percentage and heatmap showing the differentially expressed genes of four monocyte subclusters.

(C)The distribution of eleven subclusters of mononuclear phagocytes on the trajectory are shown.

(D)Heatmap showing the dynamic changes of gene expression with pseudo-time in mononuclear phagocytes.

(E)UMAP plot showing the subclusters of neutrophils. Bar plots showing the percentage.

(F)Dot plot showing correlation of scRNA-seq defined neutrophil clusters with the neutrophil subtypes reported by Chen et al.

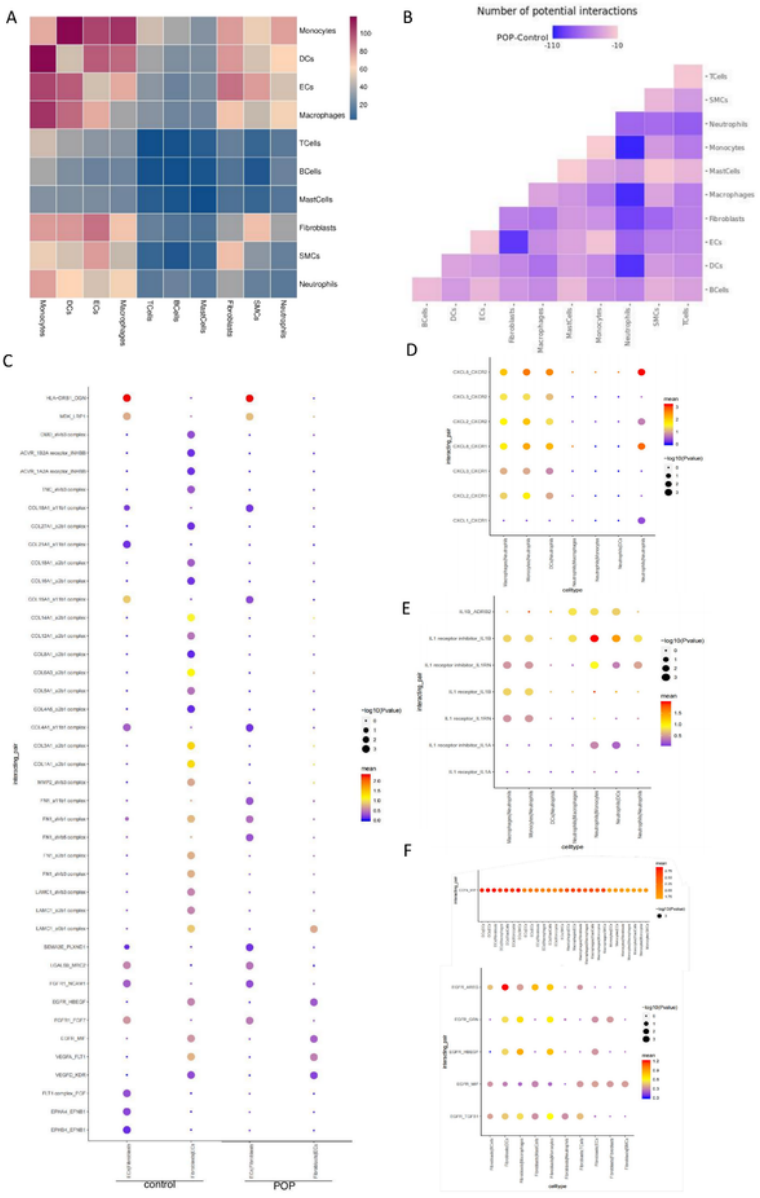


## Figure 4

Potential ligand–receptor interactions analysis in USL.

(A)Heatmap showing the numbers of cell-cell interacting pairs with each other in USL.

(B)Heatmap depicts the changed numbers of cell-cell communications in POP samples compared with control samples (all decreased).

(C)Dot plots depicting ligand–receptor pairs between fibroblasts and ECs in control sample (left) and POP samples(right). Dot size indicates the significance of the interaction and the spectrum of color represents the intensity of the interaction.

(D)Chemokines interacting pairs between neutrophils and mononuclear phagocytes in POP samples.

(E)IL-1 family interacting pairs between neutrophils and mononuclear phagocytes in POP samples.

(F)CD74-MIF and other ligand–receptor pairs in POP samples.


## Figure 5

Cell type-specific TFs and GO analysis of representative TFs.

(A)Heatmap of representative upregulated TFs in the control samples.

(B)Heatmap of representative upregulated TFs in the POP samples.

(C)Bar plots indicating the GO enrichment results of representative TFs and corresponding target genes in control samples.

(D)Bar plots indicating the GO enrichment results of representative TFs and corresponding target genes in POP samples.

## Supplementary Files

This is a list of supplementary files associated with this preprint. Click to download.

- Supplymentaryfigure.pdf